Experiments on the Richtmyer-Meshkov Instability I: Preparation of a Membraneless Interface Using the Rayleigh-Taylor Instability

Bhalchandra Puranik, Jason Oakley,
Mark Anderson, Riccardo Bonazza

September 2001

UWFDM-1171

FUSION TECHNOLOGY INSTITUTE

UNIVERSITY OF WISCONSIN

MADISON WISCONSIN

Experiments on the Richtmyer-Meshkov Instability I: Preparation of a Membraneless Interface Using the Rayleigh-Taylor Instability

Bhalchandra Puranik, Jason Oakley,
Mark Anderson, Riccardo Bonazza

Fusion Technology Institute
University of Wisconsin
1500 Engineering Drive
Madison, WI 53706

September 2001

UWFDM-1171

.

Abstract

A large number of experimental investigations of the Richtmyer-Meshkov instability (a shock-induced interfacial instability) in the past have been carried out in shock tubes. In order to separate the two gases prior to the shock arrival, a plastic membrane, on the order of one micron thick, was often used. There is considerable uncertainty regarding the effects of the membrane and membrane fragments present in the post-shock flow-field. Some investigators have attributed the lack of agreement between the experimental and numerical results to the presence of membrane fragments while some recent investigations report negligible effect of the membranes on the development of the R-M instability. Furthermore, it was postulated that for strong incident shocks, the membrane would pyrolyze and act as a continuous gaseous interface between the two gases under investigation, thus minimizing its undesirable effects. In the present experimental campaign, we investigate the interaction of strong shocks ($M > 2$) with nitrocellulose and mylar membranes. We conclude that the membrane fragments do not undergo pyrolysis and while their effects are not apparent in line-of-sight integrated optical techniques such as schlieren and shadowgraphy, they are evident when the flow-field is interrogated using a two-dimensional planar diagnostic technique. In order to create a membraneless interface, a novel technique is developed which involves retracting a thin metal plate formed into a sinusoidal shape, initially separating the two gases. Plate retraction is followed by the development of the Rayleigh-Taylor instability, leading to an interface shown by Mie scattering visualization to exhibit a repeatable, predominantly single-mode sinusoidal shape.

1 Introduction

The Richtmyer-Meshkov (R-M) instability results when a shock wave travels across a perturbed interface between two fluids. During the passage of the shock wave, vorticity is deposited at the interface due to misalignment of the pressure and density gradients (baroclinic effect). This vorticity acts as the driving mechanism for the temporal evolution of the amplitude of the perturbations present at the interface. The Richtmyer-Meshkov instability plays an important role in technological applications such as inertial confinement fusion and supersonic combustion, and in natural phenomena such as supernova core overturn. Many experimental investigations of the Richtmyer-Meshkov instability have been carried out in shock tubes. In order to create a sharp, discontinuous interface between the two gases under consideration, numerous investigators have used thin nitrocellulose or mylar membranes (thickness on the order of one micron)[1, 2, 3, 4]. The membrane could be relatively easily shaped into a sinusoidal profile by providing a suitable support frame, thus facilitating knowledge of initial amplitude and wavelength. However, membrane fragments were entrained in the flow-field following the acceleration by the incident shock wave. Results from experiments involving membranes, performed under nominally identical conditions, did not agree well with each other[2, 3]. Furthermore, the experimental results differed from the results of corresponding numerical simulations by a factor of as much as two in several cases. The discrepancy between the experimental and the numerical results was often attributed to the presence of the membrane fragments. Several investigators in recent years have tried to eliminate the presence of the membranes by developing techniques to create a membraneless interface. Benjamin and Fritz[5] studied the evolution of perturbations imposed on a membraneless interface formed by Woods metal and water that was struck by a shock wave created by the explosion of a TNT charge. Woods metal was chosen because of its very low melting point. Sinusoidal perturbations were machined on the metal surface. The metal was liquefied as the shock passed by the interface. Brouillette and Sturtevant[2, 6] and Bonazza and Sturtevant[7] carried out experiments in a vertical shock tube, wherein a membraneless diffuse interface was created by retraction of a thin metal plate separating a light gas (above the plate) from a heavy gas (below the plate), prior to the shock arrival. The plate was retracted

normal to the line of sight. Jacobs *et al.*[8, 9], Budzinski *et al.*[10] and Rightley *et al.*[11, 12] have performed R-M experiments on a shock accelerated thin layer of SF_6. The experiments were performed in a horizontal shock tube and a spatially modulated layer of SF_6 (called a gas curtain) was created inside the tube by passing the gas through a contoured nozzle vertically downward. Thus, they obtained a quasi-sinusoidal interface with finite thickness without resorting to the use of a membrane. It may be pointed out that this technique produces a two-interface configuration, rather than a classical single interface. Jacobs[13] conducted additional investigations (which do not involve a single interface) for light (He) and heavy (SF_6) shock accelerated cylinders in air. The cylinder evolves into the classical mushroom shape similar to the gas curtain experiments and the direction of evolution (upstream or downstream) is a function of the density of the cylinder gas.

Jacobs and Sheeley studied the R-M instability for two incompressible liquids in a novel apparatus[14]. The instability was generated by dropping, in a free fall, a tank containing two stratified liquids, and bouncing the tank off of a fixed coil spring. The bounce provided the impulsive acceleration. A sinusoidal shape was imparted to the interface by oscillating the container in the horizontal direction to produce standing waves. Jones and Jacobs[15] used another novel technique to obtain sinusoidal interfaces without the use of membranes. Their experiments were carried out in a vertical shock tube where an interface was formed by flowing light (N_2) and heavy (SF_6) gases from opposite ends of the shock tube. Both gases exited from opposite sides of the test section and left behind a flat stationary diffuse interface with finite thickness that was given a sinusoidal shape by gently oscillating the shock tube at a prescribed frequency in the horizontal direction.

Despite the efforts to create membraneless interfaces, the issue of membrane effects on the R-M instability has been studied extensively. Zaytsev[16] proposed that for strong incident shocks, the membrane material is pyrolyzed and acts as a continuous gaseous interface between the two gases, minimizing its effects. Recent studies[17] have concluded that the membranes have negligible effect on the development of the R-M instability if the interfacial perturbations have large amplitudes, and have significant effect only during the initial stages of the evolution if the perturbations have very small amplitudes. Thus, it can be concluded that there is considerable uncertainty regarding the effects of the membrane fragments on the

R-M instability. In the present study, we investigate the interaction of strong shock waves ($M > 2$) with nitrocellulose and mylar membranes using shadowgraphy and planar laser scattering visualizations. The objective of the present campaign is to investigate the possibility of pyrolysis of the membrane material following acceleration by strong shock waves, and to develop a technique to create a membraneless interface – if membrane fragments are found to have a significant effect on the post-shock flow-field. The experiments are performed in the new, vertical, large cross-section, high-performance Wisconsin Shock Tube[18]. R-M studies of of the new membraneless interface are discussed in the second paper of this two part series[19].

2 Experimental setup

In this section the experimental facility is introduced and the two imaging techniques are presented: shadowgraphy and planar imaging utilizing Mie scattering.

2.1 Wisconsin Shock Tube and related instrumentation

Figure 1 shows the schematic of the Wisconsin Shock Tube[18]. The shock tube is vertical, downward firing. The total height of the shock tube is 9.2 m. The driver section is round, with inner diameter of 41 cm and length of 2 m. A segment of the driven section has an outer round cross-section, 46 cm in diameter, and an inner square cross-section 25×25 cm. The driven section consists of seven such segments bolted together. These segments can be arranged in different orders, so that the mutual distances between the test section, the initial interface location and the end wall of the shock tube can be varied to study the temporal evolution of the amplitude of the interfacial perturbations. A high-pressure boost tank is connected to the driver section via a large flow rate, pneumatically driven, fast-opening valve. Piezoelectric pressure transducers are placed at various locations in the driven section to measure the speed of the shock wave and to trigger some of the controlling electronics. The interface is prepared in a special segment of the driven section, the interface section. The test section is designed to perform both line-of-sight and planar flow visualization.

A Continuum (Surelite II-PIV) pulsed Nd:YAG laser is used as a light source for imaging.

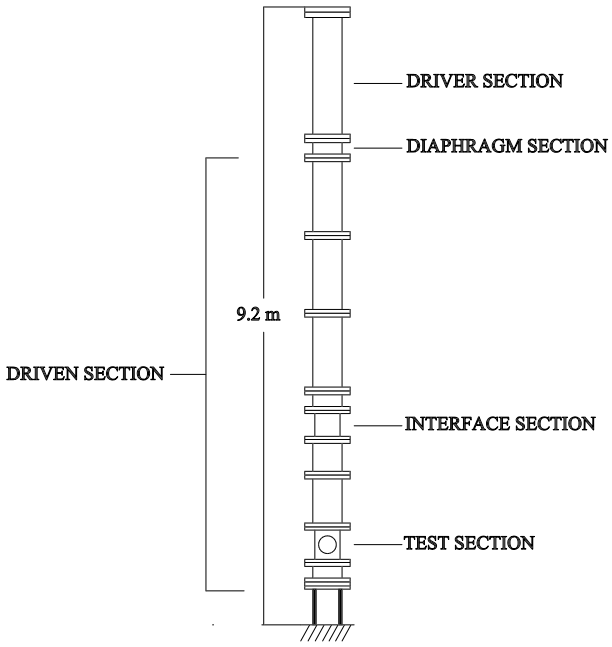

Figure 1: Schematic of the Wisconsin shock tube.

It has been modified from its original repetition mode to a "single shot" mode by suitably modifying the electronics and internal optics. The original repetition mode, as supplied by Continuum, did not allow for the laser to pulse on an external trigger. After the modifications, the capacitor bank in the laser can now be held charged by opening a reed switch placed across it and the laser is fired when a trigger signal is provided by the incident shock wave. The laser consists of two laser cavities capable of delivering 200 mJ/pulse (and hence 400 mJ/pulse when the beams are superimposed) at λ=532 nm, with a pulse width of 10 ns. A broad spectrum arc discharge lamp (Xenon Inc. Model-437B) with a pulse duration of 20 ns is used in some shadowgraphy experiments to provide a more spatially uniform light source.

A CCD camera (Spectra Video Series, by Pixel Vision) is used to capture the post-shock flow-field images. It has a back-lit, thermoelectrically cooled 1024×1024 pixel array. The camera controlling software is installed on a 250 MHz PC. A 105 mm focal length AF Nikkor Micro lens with an aperture of `f`2.8 is used with the camera. For the study of the R-T instability following the retraction of the sinusoidally shaped plate, a Spectra Physics model

2017, 5 W Ar^+ CW laser is used to illuminate the interface and a Dalsa CA-D1 256×256 pixel, 8-bit CCD camera is used to image it.

2.2 Optical diagnostic techniques

Two types of optical diagnostic techniques are used to visualize the R-M unstable interface for experiments involving membranes: shadowgraphy and planar Mie scattering. Figure 2 shows the schematic of the optical setup for shadowgraphy. The laser beam is spatially filtered before it is expanded by a plano-concave lens (focal length −15 mm). It is then collimated by a plano-convex lens (focal length 500 mm) into a parallel beam of diameter of approximately 140 mm. The collimated beam is passed through the test section windows and is projected on a screen. The CCD camera is focused on the screen and captures the image. When the arc discharge lamp is used as the light source, the spatial filter is removed from the system while keeping the same set of lenses. The shadowgraphy technique is sensitive to the second derivative of the density field which is largest near and across the interface between the two gases.

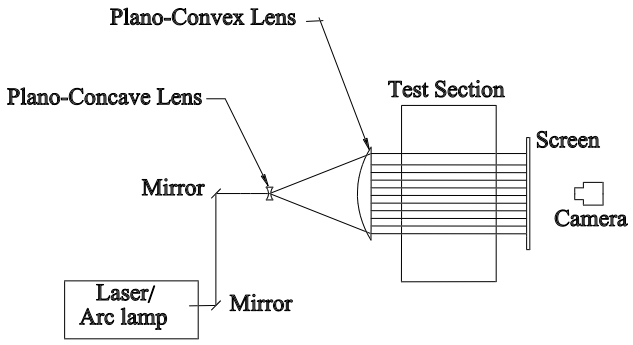

Figure 2: Optical setup for shadowgraphy imaging.

Figure 3 shows the schematic of the optical setup for planar imaging. The laser beam is expanded into a planar sheet by passing it through cylindrical optics. The beam is passed through a concave lens (focal length −33 mm) followed by a plano-convex lens (focal length 125 mm) followed by a cylindrical lens (focal length 62.5 mm) to create a sheet of desired width. It is then projected vertically upward through a 2.5 cm diameter quartz window

mounted in the bottom flange of the shock tube, such that the laser sheet is parallel to the viewing window mounted in the test section port, as shown in the schematic. The thickness and the width of the laser sheet at the center of the test section are measured to be approximately 0.3 mm and 10 cm respectively. Only one window is used for planar imaging, while an aluminum plug having identical dimensions as the window is placed in the opposing port of the test section. Using a thin laser sheet, a 2-D slice of the 3-D test section volume is interrogated, thus providing local flow information, unlike the shadowgraph technique. The CCD camera is focused on the sheet and the magnification is adjusted so that the field of view is slightly larger than the entire width of the sheet. When performing a planar Mie scattering experiment, a small amount of cigarette smoke is introduced in one of the gases (resulting in a change of Atwood number by less than 1%) and the interface is visualized by the scattering of the laser light by the smoke particles, in a direction perpendicular to the plane of the sheet. The light scattering signal from the gas which does not contain any smoke, is negligible compared to that from the gas that is seeded with smoke.

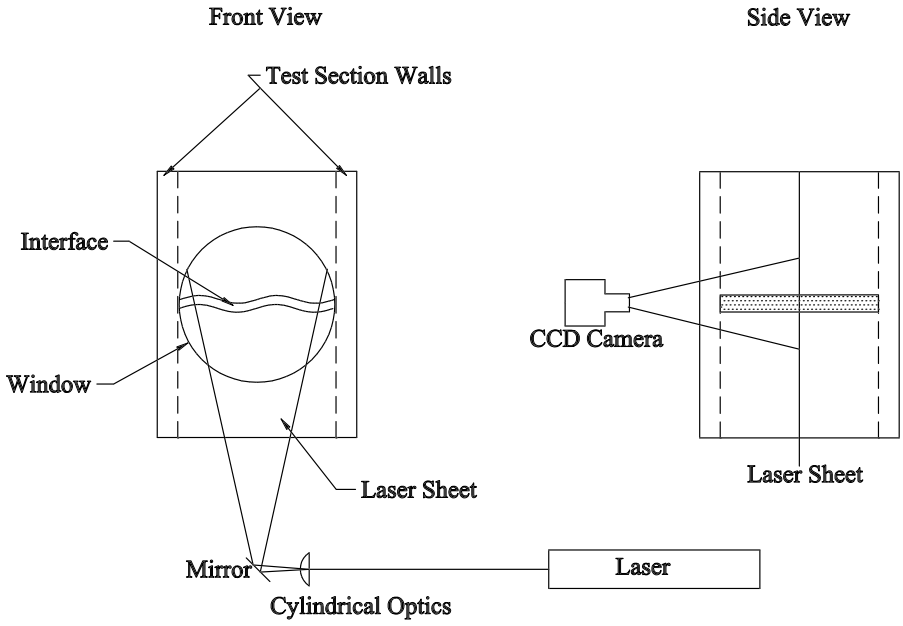

Figure 3: Optical setup for planar imaging.

3 Experiments using plastic membranes

In this section, experiments involving the use of membranes to form the interface between the two gases are described and the effects of the presence of the membrane on the R-M instability are investigated. In particular, rupture of the membrane upon shock impact is studied for strong shocks.

3.1 Membranes and support frames

Two types of membranes are investigated in this campaign: nitrocellulose and mylar. Both types of membranes are found to behave in an identical manner. All images shown in this article are of interfaces prepared with mylar membranes; the results and conclusions apply to nitrocellulose membranes as well[18]. The nitrocellulose membrane is prepared in-house while mylar is obtained commercially. To prepare a nitrocellulose membrane, a small amount (≈5 ml) of nitrocellulose solution in amyl acetate (5% or 10% strength by volume) is poured on water contained in a large shallow tank. After several seconds, the amyl acetate evaporates leaving a thin nitrocellulose membrane floating on the surface of the water. This membrane is slowly lifted using a frame made from balsa wood. It is then transferred onto an aluminum frame and allowed to dry on the aluminum frame. After drying, the frame containing the membrane is placed in the interface section of the shock tube. The thickness of the nitrocellulose membrane is approximately 0.5 μm while that of the mylar membrane is 0.94 μm. Two types of frames have been used to hold the membranes. Figures 4(a) and 4(b) show pictures of the frames used to create a flat and sinusoidal interface, respectively. The supporting surfaces of the latter are machined into a sinusoidal shape with an amplitude of 0.32 cm and a wavelength of 6.35 cm. The membrane is placed on the supporting surfaces and the two halves of the frame are bolted together to squeeze the membrane between them. A series of 0.23 mm diameter nylon monofilament wires approximately 1.27 cm apart (located at the peak, trough and approximately halfway between the peak and trough of each sine wave) are used to support and maintain the mylar film in the sine wave shape, though measurements have shown that the membrane takes on more of a sawtooth shape in the center of the frame. The wires help break apart the membrane upon shock interaction.

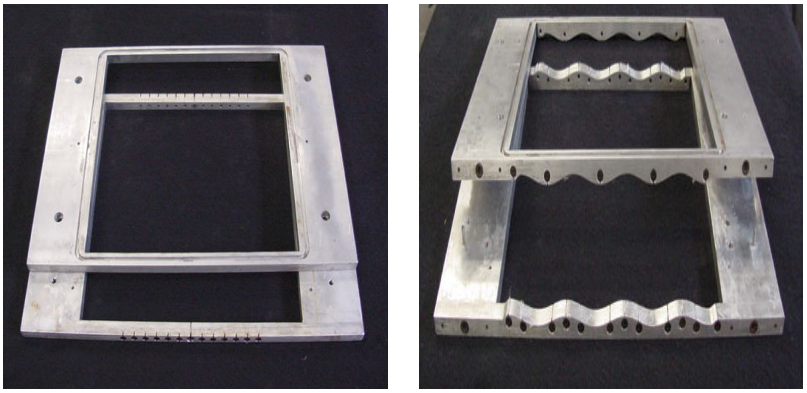

(a) (b)

Figure 4: Support frames for nitrocellulose/mylar membranes. (a): frame used to create a flat interface (b): to create a sinusoidal interface.

It is found that without the wires, the membrane tends to sag away from the sinusoidal shape in the direction perpendicular to the shaped support surfaces.

3.2 Visualization results of membrane behavior

In all images shown in this section, the direction of shock propagation is from top to bottom. Furthermore, the transmitted shock wave is out of the field of view in all images.

The experimental campaign is initiated with a flat membrane forming a nominally flat interface, with no wires used to support the membrane. Figure 5(a) shows a shadowgraph of an interface between air and argon, accelerated by a Mach 2 shock wave incident in air, 1.17 ms after the initial shock interaction. The field of view is approximately 14 cm in diameter and the laser is used as the light source. The image shows a thick dark diffuse region at the location of the interface predicted by one-dimensional gas dynamics. This image is similar to those obtained by Brouillette and Sturtevant[2]. The curved lines in the field of view are thought to be weak disturbances arising from imperfections of the inner surface of the shock tube (*e.g.* where two segments of the driven section meet and the edges of the aluminum support frame for the membrane). We believe that the dark region in the image is most likely a combination of an intact membrane that is ripped apart at the edges of the support frame and accelerated down the tube, and the interface between the two gases. The thickening of

the interface is in part due to the minute perturbations present at the pre-shock interface (due to the variation in the membrane thickness). In order to verify the inference that the image shown in Fig. 5(a) is that of an intact membrane that has traveled down the shock tube with the particle velocity behind the transmitted shock in argon, further experiments were carried out with a mylar membrane forming an air-air "interface". Physically, this means that due to the absence of a different test gas, there cannot be any R-M instability; and an intact membrane can be identified readily. Figure 5(b) shows a shadowgraph of an "interface" between air and air, accelerated by a Mach 2 shock wave, 1.05 ms after the initial shock interaction. The interface is created by a mylar membrane placed in the flat aluminum frame. It can be readily seen that the image is very similar to that of the air-argon case. The presence of the weak disturbances is evident once again. The thin, straight, inclined black line in the top portion of the image is a piece of thread placed in front of the window to check for beam collimation. The image clearly shows that the membrane indeed remains intact after the shock impact. This also shows that the images obtained using such a technique may convey incorrect information regarding the R-M growth due to the presence of the membrane. It is, therefore, concluded that it is necessary to force the membrane to rupture into smaller pieces and observe for complete annihilation of the fragments.

To rupture the membrane into smaller pieces, nine or nineteen wires (a monofilament fishing line) are placed on the aluminum support frame, in a direction perpendicular to the plane of the window (or along the line of sight). The wires, therefore, rupture the membrane into small rectangular strips upon shock impact. Figures 6(a) and (b) show two shadowgraph images of a nitrogen-nitrogen "interface", accelerated by a Mach 2.83 shock wave, 623 μs after the shock interaction. Note that the Mach number of the shock wave is considerably higher compared to the cases described previously. The arc discharge lamp is used as the light source for both cases. Wires are placed at a separation distance of 2.54 cm in Fig. 6(a) and at a distance of 1.27 cm in Fig. 6(b). It can be observed from the images that the wires indeed rupture the membrane into several small fragments which are all present at the interface location predicted by one-dimensional gas dynamics. The thin dark region in the upper right portion of the field of view is a defect that developed in one of the viewing windows. From these images, we see that even though the membrane is ruptured into small pieces, it is still not pyrolyzed at strong shocks.

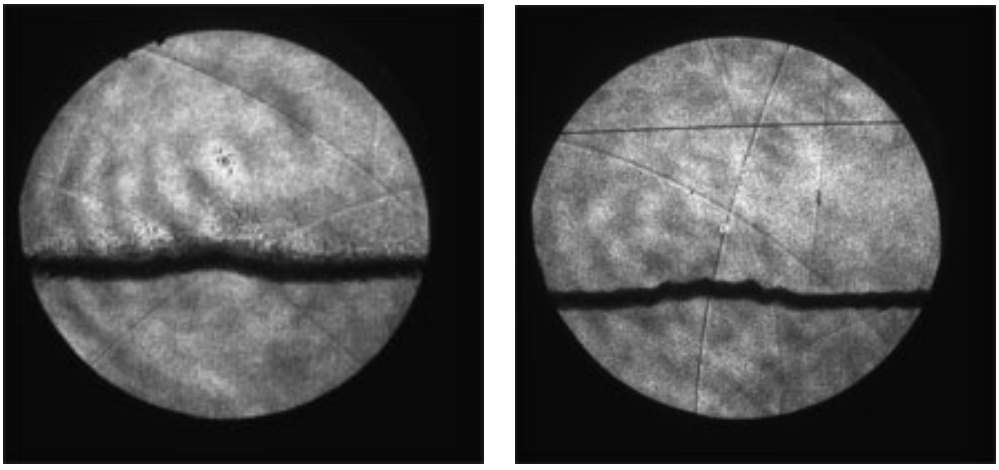

(a) (b)

Figure 5: (a) Shadowgraph image of an initially flat air-argon interface formed using a mylar membrane, 1.17 ms after interaction with a Mach 2 shock wave incident in air. (b) Shadowgraph image of an initially flat air-air "interface" formed using a mylar membrane, 1.05 ms after interaction with a Mach 2 shock wave.

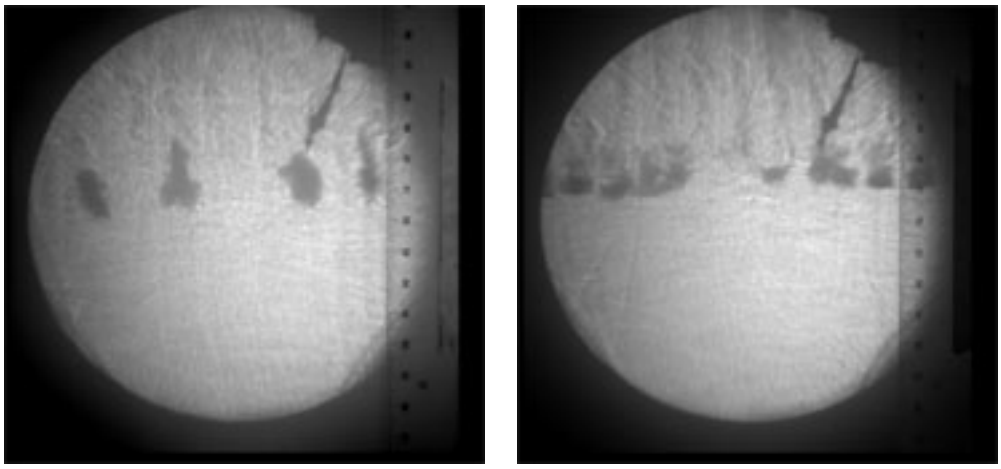

(a) (b)

Figure 6: Shadowgraph images of an initially flat N_2-N_2 "interface", 623 μs after interaction with a Mach 2.83 shock wave. The interface is formed by a mylar membrane supported by several wires with a spacing of 2.54 cm for (a) and 1.27 cm for (b).

In order to further investigate the effects of the membrane fragments on the R-M instability, planar Mie scattering imaging is employed. Figures 7(a) and (b) show planar images of the growth of a sinuous interface between helium and CO_2, accelerated by a Mach 2.08 shock wave, 738 μs and 1.23 ms, respectively, after the shock interaction. The CO_2 (the test gas at the bottom) is seeded with cigarette smoke. The membrane fragments are clearly seen in both images as the bright areas at the peaks and troughs of the originally sinuous interface. Due to the high Atwood number associated with the helium-CO_2 interface (0.867, post-shock), the instability rapidly grows into the nonlinear regime. The spikes of CO_2 interleaved by the flat bubbles of helium are seen in both images.

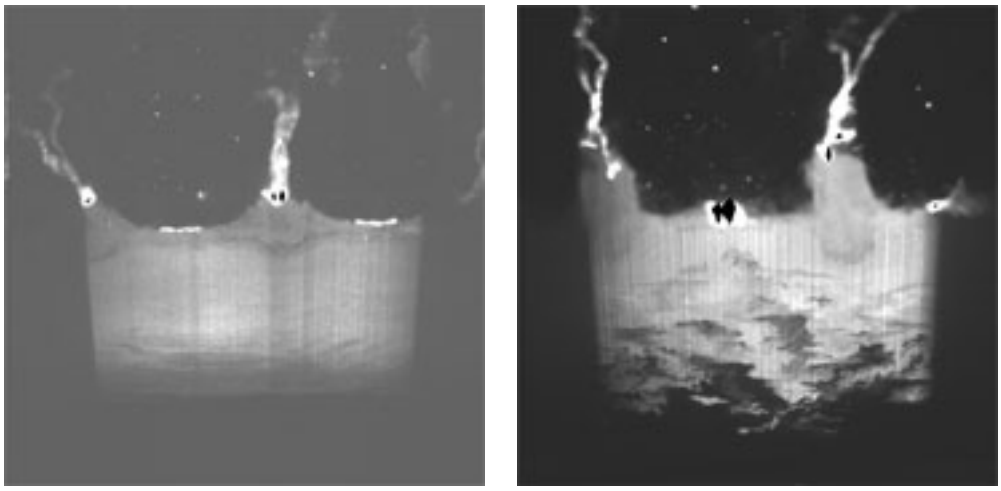

(a) (b)

Figure 7: Planar Mie scattering images of an initially sinusoidal helium-CO_2 interface, 738 μs (a) and 1.23 ms (b) after interaction with a Mach 2.08 shock wave incident in helium. The interface is formed by a mylar membrane supported by several wires.

In Fig. 7(a), the membrane fragments at the trough locations are fairly flat, while those at the peak locations are squeezed into the CO_2 spikes. However, at the later time, as seen in Fig. 7(b), the fragments appear to start disrupting the flow patterns. In particular, the fragment in the trough position at the left appears to drag some CO_2 upward and the fragment at the peak position might be hampering the Kelvin-Helmholtz roll-ups that are characteristic of the late time behavior. Such details are hidden in the case of diagnostic techniques such as shadowgraphy or schlieren which provide line-of-sight-integrated information, and

might lead to erroneous conclusions regarding growth rates. The planar images that provide local flow information show the details of the membrane effects quite clearly. Therefore, we conclude that the presence of membrane fragments is undesirable; however, increasing the number of wires would result in breakup of the membrane into smaller fragments which could significantly reduce the effects of the turbulence.

4 Creation of membraneless interface

In this section, we describe experiments performed to achieve a membraneless interface in order to eliminate the presence of the membrane fragments.

4.1 Sinusoidally shaped retractable plate

In an effort to impose known repeatable perturbations on a membraneless interface, a sinusoidally shaped retractable plate is manufactured. Figure 8 shows a picture of the sinusoidal plate and the frame in which it slides. The plate is made by forming a 0.58 mm thick copper sheet into a sinusoidal shape in the central part that merges with the flat outside part in a smooth transition. The flat portion of the plate slides into a slot machined in the aluminum support frame. To form the copper plate into a sinusoidal shape, it is passed through a custom built pair of steel rollers shown in Fig. 9. The shape on the plate consists of two full wavelengths of the sinusoid in the central portion. The wavelength (λ) and the amplitude (η) of the perturbation thus imposed on the plate are 38.1 mm and 3.18 mm respectively, giving rise to an amplitude to wavelength ratio (η/λ) of 0.083. When impulsively accelerated, an interface with this geometry will very quickly enter the nonlinear stages of the R-M instability (see part II of this series[19]).

4.2 Characterization of initial conditions

As a first step in the campaign with the sinusoidal plate, initial condition characterization studies are carried out in the test section of the shock tube. Figure 10 shows the schematic of the setup for this purpose. The sinusoidal plate is inserted in the test section of the shock

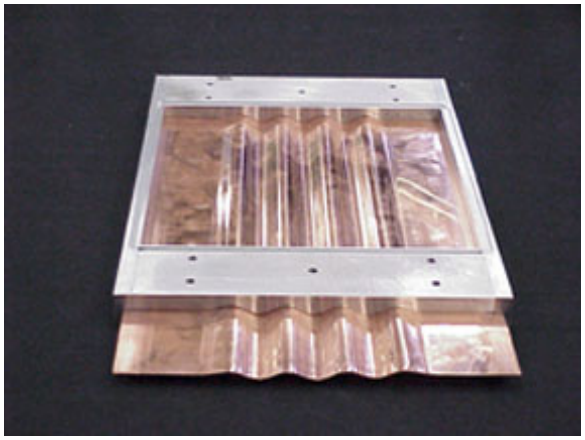

Figure 8: Sinusoidally shaped copper plate and support frame.

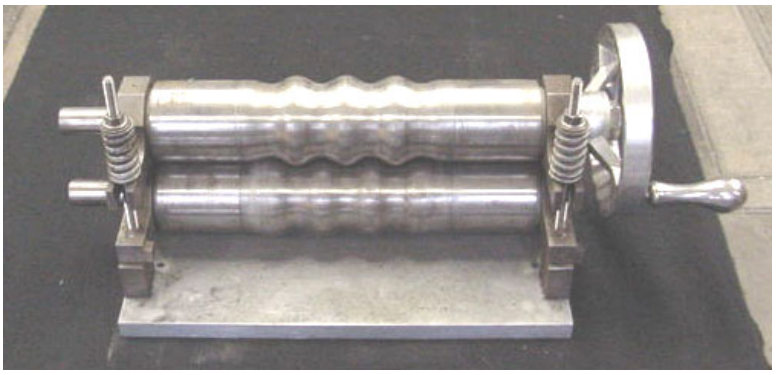

Figure 9: Steel rollers used to form the copper plate into a sinusoidal shape. The surfaces of the rollers are machined into a sinusoidal profile on a CNC lathe.

tube. Two different gases are introduced above and below the plate. A continuous wave Ar^+ laser illuminates the test section. The laser beam is expanded into a planar sheet using cylindrical optics and projected vertically upward through the small quartz window in the bottom flange of the shock tube, parallel to the test section window. The position of the sheet is adjusted so that the sinusoidal portion of the retractable plate that includes the two wavelengths of the profile is illuminated. A small amount of cigarette smoke is introduced in one of the gases and the Mie scattering signal off the smoke particles is collected in a direction at right angles to the plane of the laser sheet with a CCD camera.

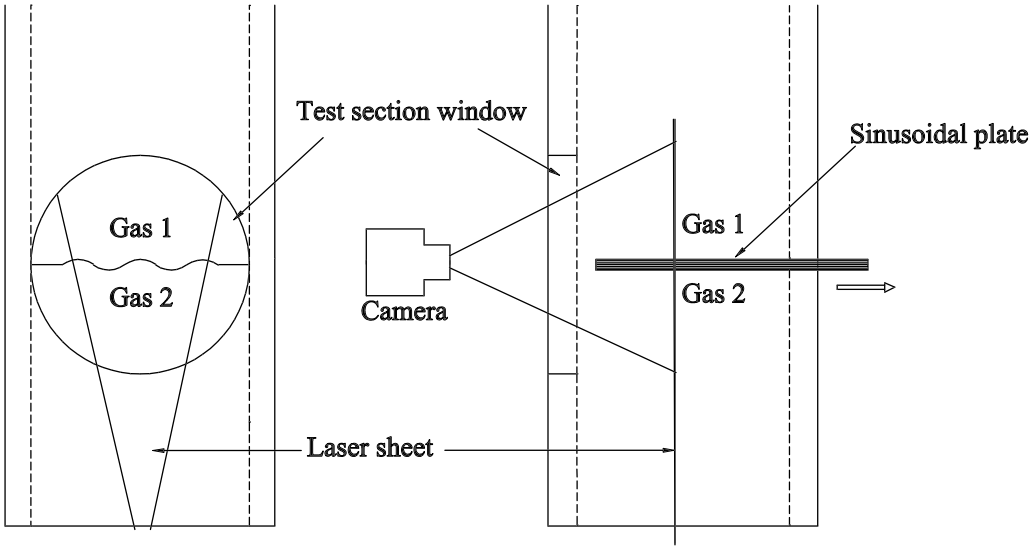

Figure 10: Schematic of the setup for characterization of initial conditions formed by the sinusoidal retractable plate. The direction of retraction is along the line of sight.

4.2.1 Light/heavy configuration

In this section, experiments with light gas over heavy gas with the sinusoidal plate initially separating the two are discussed. Figures 11(a)-(p) show a series of images of the retraction process, with helium above air. Air is seeded with a small amount of smoke. Images are captured at a rate of 100 frames per second.

Image (a) shows the two gases separated by the sinusoidal plate. The plate retraction process has not begun yet. Image (b) is captured approximately at the time when the plate, while retracting, has just crossed the plane of the laser sheet. We call this the initial time, t=0, since the two gases come in contact with each other for the first time in the plane of the laser sheet. Some smoke seems to have risen and can be seen within the helium. We believe this smoke is not in the plane of the laser sheet but is visible due to reflections of the laser light within the test section. Image (c) is captured at time t=10 ms. The sinusoidal edge of the retracting plate is clearly visible in the image. Some smoke has risen in the initial trough locations, thus making the interface depart from its original sinusoidal profile into a flat profile. Image (d) shows the development of the process at t=50 ms. The sinusoidal

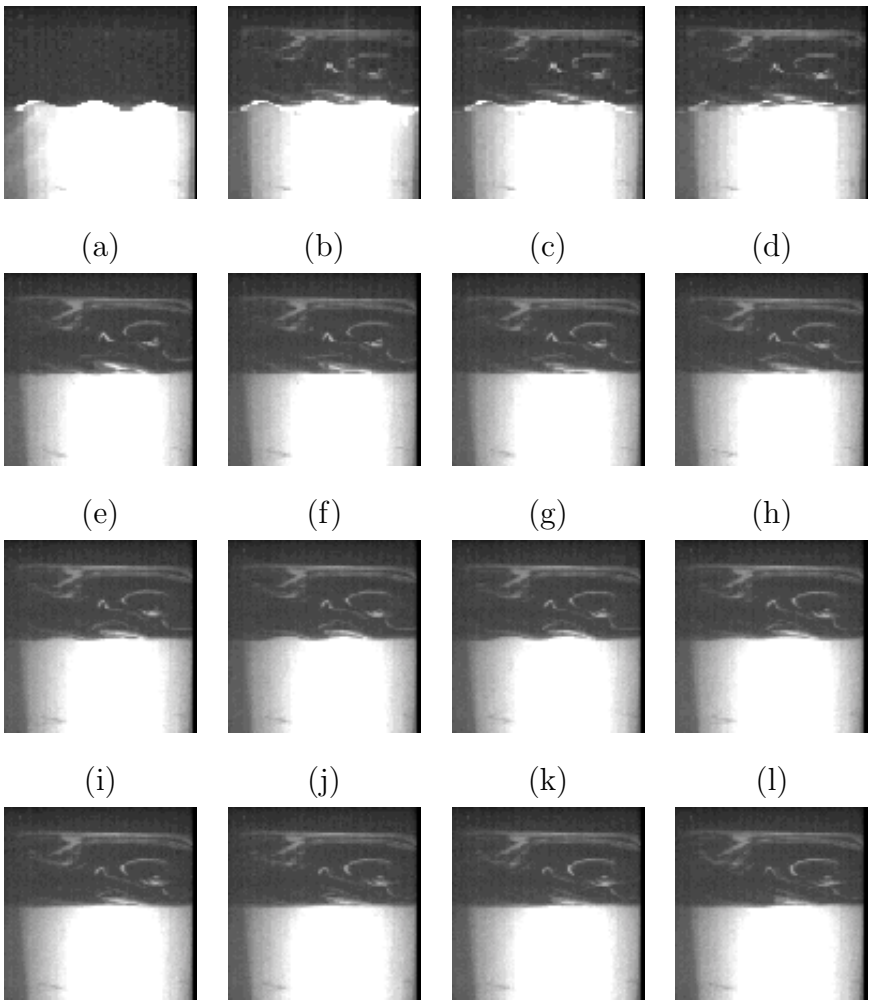

Figure 11: Series of images showing the formation of membraneless interface between helium and air by retraction of the corrugated plate. The images are captured at the following times: (a) 0^- ms, (b) 0^+ ms, (c) 10 ms, (d) 50 ms, (e) 100 ms, (f) 150 ms, (g) 200 ms, (h) 250 ms, (i) 300 ms, (j) 350 ms, (k) 400 ms, (l) 450 ms, (m) 500 ms, (n) 550 ms, (o) 600 ms, (p) 650 ms.

edge of the retracing plate and the interface are seen to be out of phase by approximately 90°. This indicates the presence of flow oscillation. Indeed, with the light fluid on top of heavy fluid, Rayleigh-Taylor theory predicts the formation of standing waves at the interface between the two. A crest is seen to form at an original trough location and vice versa. Image (e) shows the process at t=100 ms. The crests and troughs are in the same locations as seen

in (d); however, their amplitudes seem smaller than in (d), indicating the damping of the oscillations. Image (f) shows the process at t=150 ms. The crests and troughs seen in (d) and (e) have flattened out. Images (g)-(p) show the later states of the interface at 50 ms intervals, with (g) corresponding to t=200 ms. It can be seen from the images that the oscillations slowly die, leaving the interface nominally flat after t=500 ms.

For the light/heavy experiments, the flow oscillation phenomenon is observed with a decreasing amplitude until the perturbations formed at the interface by the sinusoidal plate flatten out. Furthermore, the amplitude of the perturbations becomes extremely small in a very short amount of time, thus making the amplitude to wavelength ratio very small. For the desired R-M studies, a near nonlinear initial condition is desired, and therefore, it is concluded that the light/heavy configuration does not provide the necessary initial condition. However, the light/heavy configuration may prove useful for studies of a nearly flat interface where thermal diffusion can be a controlled variable by delaying the incident shock arrival.

4.2.2 Heavy/light configuration

In this section, experiments with heavy gas over light gas with the sinusoidal plate initially separating the two are discussed. This configuration produces the Rayleigh-Taylor instability, since the light fluid supports a heavy fluid against the constant acceleration of gravity. Figures 12(a)-(p) shows a series of images of the development of the Rayleigh-Taylor instability with CO_2 above air. Air is seeded with a small amount of smoke. The images are captured at a rate of 100 frames per second.

Image (a) shows the beginning of the retraction process, with CO_2 above air with the plate separating the two. Image (b) is captured when the plate, while retracting, is crossing the plane of the laser sheet. We call this the initial time, t=0, since the R-T instability begins to grow in the plane of the laser sheet at this instant. Images (c)-(n) show the development of the instability, with the time between successive images being 10 ms. It can be seen from the images that the two fluids continue to penetrate each other and the amplitude of the perturbation increases until t=120 ms, while the wavelength remains approximately constant. At this time, secondary Kelvin-Helmholtz instabilities set in, resulting in vortex roll-ups (mushroom structures), indicating highly nonlinear growth. This can be seen in

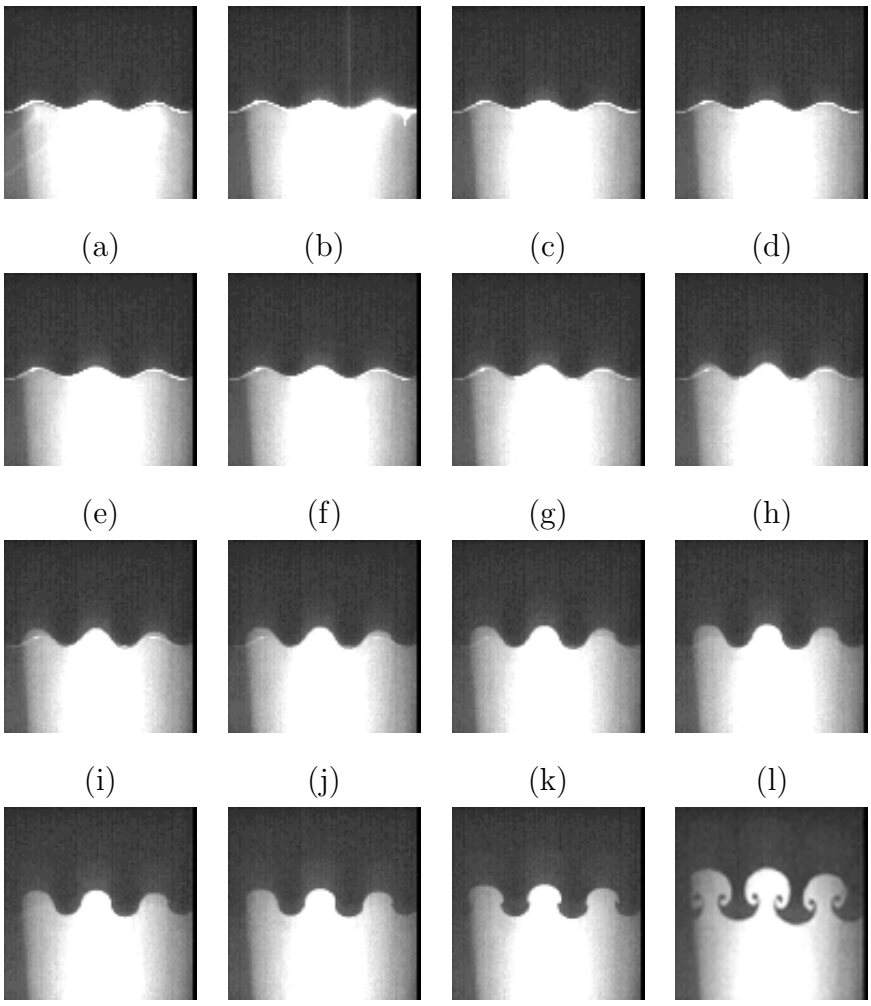

Figure 12: Series of images showing the formation of membraneless interface between CO_2 and air by retraction of the corrugated plate. The images are captured at the following times: (a) 0^- ms, (b) 0^+ ms, (c) 10 ms, (d) 20 ms, (e) 30 ms, (f) 40 ms, (g) 50 ms, (h) 60 ms, (i) 70 ms, (j) 80 ms, (k) 90 ms, (l) 100 ms, (m) 110 ms, (n) 120 ms, (o) 150 ms, (p) 250 ms.

images (o) and (p) corresponding to t=150 ms and t=200 ms, respectively. However, the mushrooms are seen growing independently and do not interact with each other until very late. At extremely late times (images not shown here), however, adjacent mushrooms interact with each other resulting in a turbulent mixing of the two gases. It can be noted that the flow-field appears remarkably two-dimensional in the sequence of images shown. The plate,

while retracting, drags with it a certain amount of fluid that bounces back off the shock tube wall and eventually introduces three-dimensional effects. However, until the time shown in image (p), the flow-field remains fairly two-dimensional. The growth of each perturbation is seen to be symmetrical until the later times, as in image (p), where the mushroom structures appear to be tilting. The tilting is attributed to the finite number of wavelengths (shown in Fig. 8) in the finite width of the test section. A theoretical infinite number of perturbations would ideally all grow symmetrically.

This experiment is repeated several times and it is observed that the growth of the Rayleigh-Taylor instability is visually consistent each time. Furthermore, the instability is seen to remain two-dimensional until very late stages of evolution. It is observed that the perturbation remains approximately sinusoidal until $t \approx 120$ ms; the secondary K-H instabilities appear at this time. Therefore, if the plate is fully retracted out of the shock tube within approximately 100 ms after crossing the plane of the laser sheet, the R-T instability developed at the interface presents a useful initial perturbation for the R-M instability. The interface is very sharp due to insufficient time for diffusion to have any visible effect; it is two-dimensional with a sinusoidal shape and there is no membrane utilized to create the interface.

In order to quantify the shape of the R-T developed interface and estimate the amplitude of the perturbations at various times during the R-T growth, an edge detection algorithm is developed. Figure 13 shows a plot of pixel values versus the ordinate, for a given abscissa in an image. From the figure, it can be seen that the pixel values are very small in the top portion of the image, indicating pure, unseeded CO_2. The pixel values increase in the bottom portion of the image, indicating smoke-seeded air. The appropriate transition point for the pixel values determines the location of the interface at the abscissa location under consideration. The locus of all interface locations gives the shape of the interface.

The appropriate transition point in the pixel value profile is calculated as proposed by Bonazza and Sturtevant[7]:

$$y = \frac{\int_0^Y P(y)dy}{M - m}, \tag{1}$$

where $P(y)$ is the pixel value at any y location, Y is the height of the field of view in the image and M and m are the maximum and minimum asymptotic pixel values in the

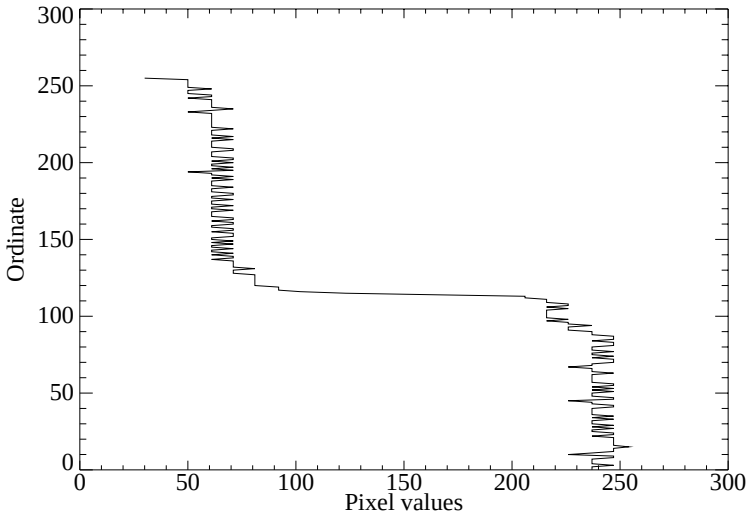

Figure 13: An example of profile of pixel values at a given abscissa.

profile, respectively. M and m represent the scattering signal from air (seeded with smoke particles) and CO_2 respectively. M and m are determined by averaging over 70 pixel values in the bottom and top regions of the image respectively. To carry out a modal analysis of the interface shape, its spatial spectrum is constructed by an FFT. A spatial region encompassing two full wavelengths of the perturbation is selected for the Fourier analysis. A low pass digital filter is applied in the frequency domain and a smooth interface is reconstructed using only the first six modes of the spectrum. An explicit mathematical expression is formed from the FFT information to describe the interface shape. Figure 14 shows an example of the extracted interface shape superimposed on the smooth reconstructed shape, for t=110 ms.

Table 1 lists the modal amplitudes, phases and modal amplitude standard deviations (as measured over 10 experiments) for the six-term Fourier series representation of the interface shape for t=0-120 ms. The series used to represent the interface is:

$$y = \sum_{i=1}^{6} \eta_i \cos\left(\frac{2\pi}{\lambda} ix + \phi_i\right), \tag{2}$$

where y is the amplitude, i is the coefficient number, η_i and ϕ_i are the modal amplitude and phase angles respectively, λ=76.2 mm, and $x \in [0, 76.2 \text{ mm}]$. Note that after t=120 ms, the formation of mushroom structures results in an interface with multiple values for a given abscissa. Thus, Fourier transformation of such a shape is not possible (a wavelet

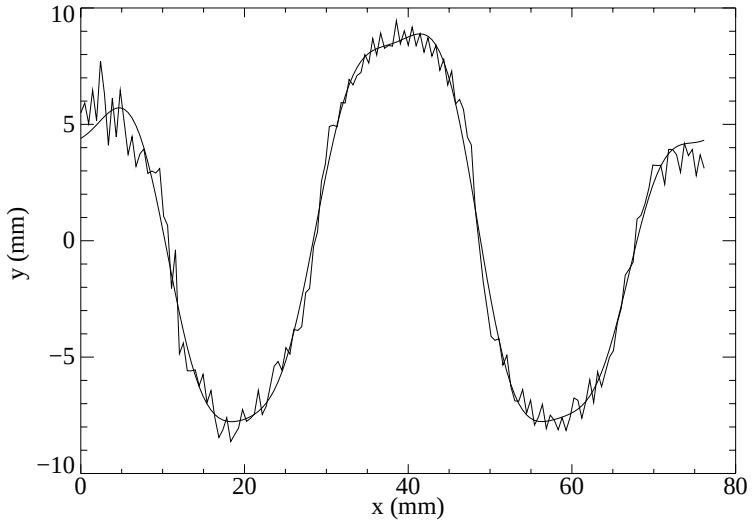

Figure 14: Smooth reconstructed interface shape superimposed on the extracted interface shape for t=110 ms. Note that two wavelengths in the central portion of the image are chosen as the region of interest.

description of the interface geometry may be possible). The small values of the standard deviations (at least in regard to mode 2) suggest that the development of the instability is fairly consistent and the repeatability of the formation of an interface shape at any given time is quite acceptable.

Figure 15 shows the superposition of the reconstructed interface shapes for t=10-120 ms, demonstrating the growth of the R-T instability. Figure 16 shows the modal amplitude growth for the first six modes until t=120 ms. It can be seen that the second mode (fundamental mode) is the most dominant, with its amplitude very close to the total amplitude of the perturbation. Therefore, the formation of a nearly single mode sinusoidal interface is verified quantitatively.

The experimentally measured R-T amplitude growth is compared with existing theories. The classical R-T expression for the growth of the amplitude of sinusoidal perturbations given by Lord Rayleigh[20] is:

$$\eta(t) = \eta_0 \exp\left(\sqrt{kgA}\, t\right) \tag{3}$$

The above expression is valid in the linear regime of growth ($\eta \ll \lambda$). Several analyses and

Time (ms)		Mode 1	Mode 2	Mode 3	Mode 4	Mode 5	Mode 6
0	η_i (mm)	0.00	3.18	0.00	0.00	0.00	0.00
	ϕ_i (rad)	0.00	0.00	0.00	0.00	0.00	0.00
	σ_i (mm)	0.00	0.00	0.00	0.00	0.00	0.00
10	η_i (mm)	0.89	3.56	0.15	0.21	0.10	0.11
	ϕ_i (rad)	-2.96	-0.04	-1.03	-1.38	-1.53	-2.16
	σ_i (mm)	0.15	0.26	0.08	0.11	0.05	0.04
20	η_i (mm)	0.94	3.74	0.18	0.25	0.12	0.14
	ϕ_i (rad)	-2.97	-0.04	-1.19	-1.46	-1.93	-2.76
	σ_i (mm)	0.16	0.26	0.08	0.13	0.05	0.05
30	η_i (mm)	0.99	3.99	0.19	0.27	0.13	0.17
	ϕ_i (rad)	-3.00	-0.06	-1.31	-1.56	-2.07	-2.77
	σ_i (mm)	0.13	0.26	0.11	0.10	0.04	0.04
40	η_i (mm)	1.01	4.39	0.21	0.31	0.13	0.23
	ϕ_i (rad)	-3.02	-0.06	-1.48	-1.52	-2.32	-2.94
	σ_i (mm)	0.15	0.27	0.10	0.09	0.05	0.05
50	η_i (mm)	1.07	4.86	0.19	0.36	0.15	0.28
	ϕ_i (rad)	-3.04	-0.08	-1.42	-1.77	-2.42	-2.95
	σ_i (mm)	0.17	0.24	0.08	0.10	0.08	0.05
60	η_i (mm)	1.11	5.41	0.22	0.42	0.15	0.34
	ϕ_i (rad)	-2.99	-0.08	-1.72	-1.86	-2.79	-3.08
	σ_i (mm)	0.18	0.27	0.11	0.11	0.06	0.06
70	η_i (mm)	1.12	6.03	0.25	0.44	0.15	0.39
	ϕ_i (rad)	-2.96	-0.08	-2.25	-2.09	-2.70	-3.05
	σ_i (mm)	0.18	0.31	0.11	0.12	0.06	0.08
80	η_i (mm)	1.22	6.65	0.35	0.50	0.17	0.51
	ϕ_i (rad)	-2.92	-0.09	-2.62	-2.32	-2.56	-3.12
	σ_i (mm)	0.16	0.30	0.17	0.16	0.10	0.09
90	η_i (mm)	1.32	7.22	0.50	0.54	0.15	0.64
	ϕ_i (rad)	-2.92	-0.09	-2.81	-2.55	-3.11	-3.09
	σ_i (mm)	0.21	0.30	0.16	0.20	0.11	0.10
100	η_i (mm)	1.43	7.82	0.61	0.59	0.15	0.83
	ϕ_i (rad)	-2.96	-0.09	-2.99	-2.50	-2.63	-3.14
	σ_i (mm)	0.26	0.38	0.18	0.24	0.12	0.14
110	η (mm)	1.42	8.45	0.66	0.68	0.18	0.99
	ϕ_i (rad)	-2.97	-0.10	-2.93	-2.69	-2.24	-2.98
	σ_i (mm)	0.30	0.49	0.19	0.30	0.13	0.16
120	η_i (mm)	1.40	9.13	0.74	0.79	0.23	1.15
	ϕ_i (rad)	-3.00	-0.08	-2.93	-2.78	-2.35	-3.03
	σ_i (mm)	0.31	0.51	0.22	0.33	0.17	0.18

Table 1: Modal amplitudes and phase angles for times of growth up to 120 ms, averaged over ten experiments, along with the amplitude standard deviations (σ_i).

models for the description of the nonlinear regime have been proposed in which the growth is described in terms of the depth of penetration of the lighter fluid into the heavier one, h.

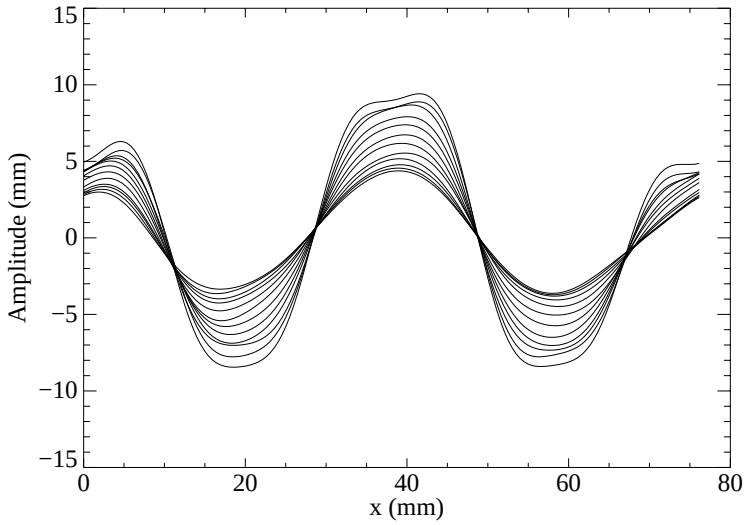

Figure 15: Superposition of reconstructed interface shapes for t=0-120 ms showing the growth of the R-T instability.

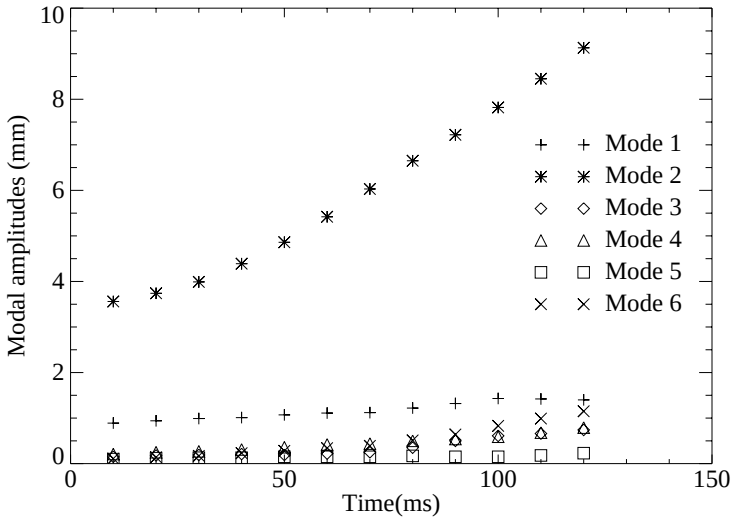

Figure 16: Comparative amplitudes for the first six modes.

For a single mode perturbation, Alon *et al.*[21] have proposed a balance of buoyancy and drag at the bubble tip which predicts:

$$h \sim \sqrt{\frac{2A}{1+A} g\lambda}\, t \ . \tag{4}$$

The most widely accepted law in the case of a multimode or random perturbation is given by Read[22] as:

$$h = \alpha A g t^2, \tag{5}$$

where α is determined experimentally and is $\approx$0.07. The Atwood number (A) in the present case is 0.206 and g=9.81 m/s^2. Figure 17 compares the experimentally measured growth for the most dominant mode (Mode 2) with the linear and multimode nonlinear[22] growth expressions. The comparison shows that the linear law considerably overpredicts the growth. This is, however, expected due to the fact that the perturbation grows quickly out of the linear regime (*e.g.* $\eta/\lambda = 0.11$ at t=10 ms). The multimode nonlinear law[22] underpredicts the growth, especially at later times. This can be explained on the basis of the fact that the amplitudes of the higher modes present in the perturbation are almost an order of magnitude smaller than that of the most dominant mode. Figure 18 shows a comparison of the experimentally measured bubble penetration height with the prediction from the multimode nonlinear R-T law[22]. Note that the peak bubble penetration depth is similar in behavior, but slightly higher than, the amplitude of the most dominant mode shown in Fig. 16. It is measured by finding the peak amplitude of the interface at successive growth times. It can be seen that, once again, the multimode nonlinear R-T law[22] underpredicts the growth.

Figure 19 shows the comparison of the experimentally measured bubble penetration height and amplitude for the most dominant mode (Mode 2) with the prediction from the single mode nonlinear R-T law[21] using a constant of proportionality equal to $1/2\pi$. The choice of the constant is based on the prescription given by Sadot *et al.*[23] for asymptotic growth rate of a R-M bubble for low Atwood numbers. It can be seen from the figure that the experimental bubble penetration depth measurements agree well with the prediction from the single mode nonlinear law.

5 Conclusion

An investigation, involving the use of thin mylar or nitrocellulose membranes to form an interface between two gases, is carried out to study the effects of membranes on the R-M

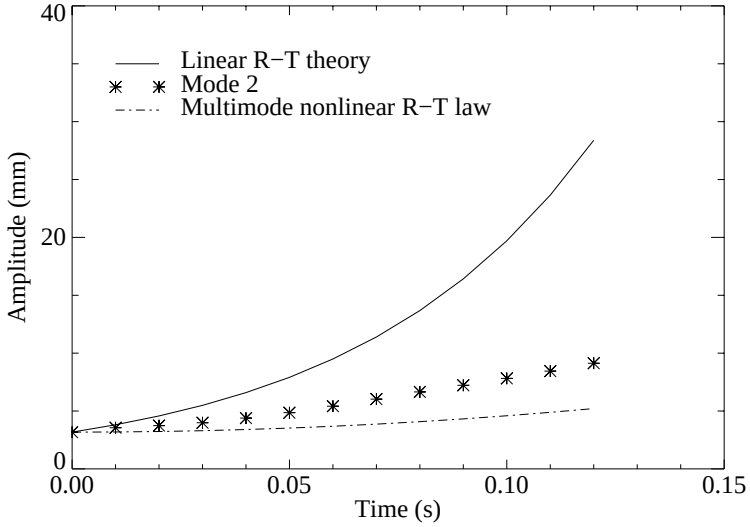

Figure 17: Comparison of experimentally measured amplitude of the most dominant mode with the linear R-T theory and multimode nonlinear R-T law.

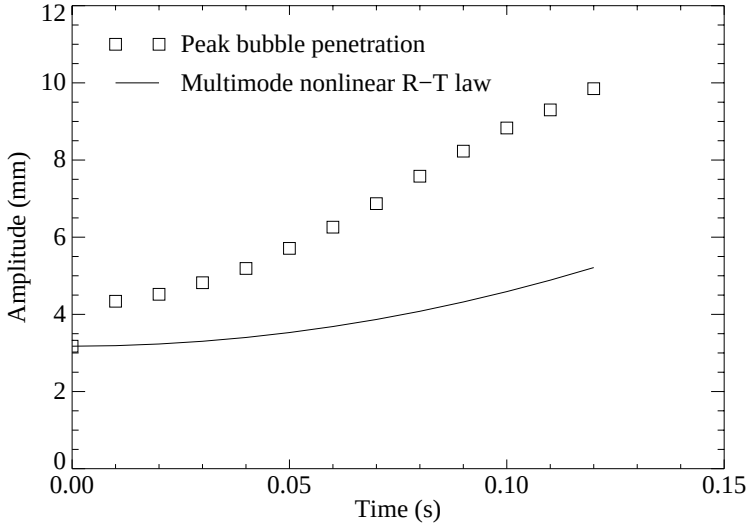

Figure 18: Comparison of experimentally measured peak bubble penetration height with the multimode nonlinear R-T law.

instability. It is found that without use of support wires, the membrane is ripped at its edges and remains intact as one piece that travels with the interface behind the transmitted shock. This is consistent with observations from previous investigations. When the membrane is

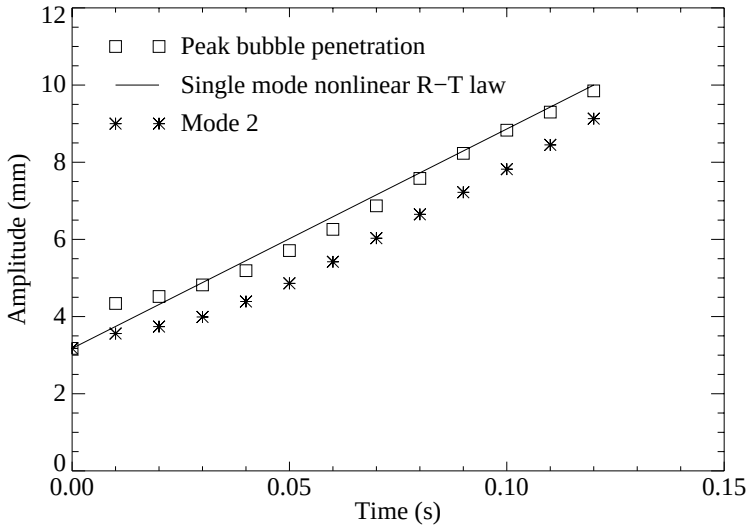

Figure 19: Comparison of experimentally measured peak bubble penetration height and amplitude of the most dominant mode with the single mode nonlinear R-T law.

ruptured into several small pieces using support wires, the fragments are observed to remain intact and are found to be present at the interface location. For incident shock strengths up to Mach 3, pyrolysis of the membrane fragments is not observed. The membrane fragments are thought to affect the growth patterns of the instability, particularly in the nonlinear regime. It is therefore concluded that a membraneless interface is essential for studying the R-M instability in its purest form.

To create a membraneless interface, a novel technique is developed. A thin metal sheet, formed into a sinusoidal shape initially separating the two gases of interest, is retracted to form the interface. When a light fluid is present above a heavy fluid, the initial perturbations formed at the interface are observed to undergo oscillatory behavior and die out quickly due to damping as well as dispersion. When a heavy fluid is present over a light fluid, the amplitude of an initial perturbation grows due to the Rayleigh-Taylor instability. It is found that for the combination of CO_2 above air, the perturbations grow maintaining a sinusoidal profile up to approximately 120 ms after the two gases come in contact with each other. The flow-field is found to be predominantly two-dimensional and the Rayleigh-Taylor developed interface presents a useful nonlinear initial perturbation for a Richtmyer-Meshkov

experiment. Fourier analysis of the R-T-developed interface shows that the interface is sinusoidal with one dominant mode. The plate retraction technique is further modified to a two stage process and an R-M experiment to accelerate the R-T-developed interface by a Mach 3.08 shock wave incident in CO_2 is designed; the results of the R-M experiments are described in a companion article[19].

References

[1] Ye. Ye. Meshkov. Instability of a shock wave accelerated interface between two gases. *NASA Technical Translation, NASA TT F-13,074*, 1970.

[2] M. Brouillette and B. Sturtevant. Experiments on the Richtmyer-Meshkov instability: Small-scale perturbations on a plane interface. *Phys. Fluids A*, 5(4):916–930, 1993.

[3] L. Houas and I. Chemouni. Experimental investigation of Richtmyer-Meshkov instability in shock tube. *Phys. Fluids*, 8(2):614–627, 1996.

[4] G. Jourdan, L. Houas, J. F. Haas, and G. Ben-Dor. Thickness and volume measurements of a Richtmyer-Meshkov instability-induced mixing zone in a square shock tube. *J. Fluid Mech.*, 349:67–94, 1997.

[5] R. F. Benjamin and J. N. Fritz. Shock loading a rippled interface between liquids of different densities. *Phys. Fluids*, 30(2):331–336, 1987.

[6] M. Brouillette and B. Sturtevant. Experiments on the Richtmyer-Meshkov instability: Single-scale perturbations on a continuous interface. *J. Fluid Mech.*, 263:271–292, 1994.

[7] R. Bonazza and B. Sturtevant. X-ray measurements of growth rates at a gas interface accelerated by shock waves. *Phys. Fluids*, 8(9):2496–2512, 1996.

[8] J. W. Jacobs, D. L. Klein, D. G. Jenkins, and R. F. Benjamin. Instability growth patterns of a shock-accelerated thin fluid layer. *Phys. Rev. Let.*, 70(5):583–586, 1993.

[9] J. W. Jacobs, D. G. Jenkins, D. L. Klein, and R. F. Benjamin. Nonlinear growth of the shock-accelerated instability of a thin fluid layer. *J. Fluid Mech.*, 295:23–42, 1995.

[10] J. M. Budzinski, R. F. Benjamin, and J. W. Jacobs. Influence of initial conditions on the flow patterns of a shock-accelerated thin fluid layer. *Phys. Fluids*, 6(11):3510–3512, 1994.

[11] P. M. Rightley, P. Vorobieff, and R. F. Benjamin. Evolution of a shock-accelerated thin fluid layer. *Phys. Fluids*, 9(6):1770–1782, 1997.

[12] P. Rightley, P. Vorobieff, R. Benjamin, and R. Martin. Experimental observation of the mixing transition in a shock-accelerated gas curtain. *Phys. Fluids*, 1988. submitted Mar. 3.

[13] J. W. Jacobs. The dynamics of shock accelerated light and heavy gas cylinders. *Phys. Fluids A*, 5(9):2239–2247, 1993.

[14] J. W. Jacobs and J. M. Sheeley. Experimental study of incompressible Richtmyer-Meshkov instability. *Phys. Fluids*, 8(2):405–415, 1996.

[15] M. A. Jones and J. W. Jacobs. A membraneless experiment for the study of Richtmyer-Meshkov instability of a shock-accelerated gas interface. *Phys. Fluids*, 9(10):3078–3084, 1997.

[16] S. G. Zaytsev, E. V. Lazareva, V. V. Chernuka, and V. M. Belyaev. Intensification of mixing at the interface between media of different densities upon the passage of a shock wave through it. *Dolk. Akad. Nauk. SSSR*, 283:94–98, 1985.

[17] L. Erez, O. Sadot, D. Oron, G. Erez, L. A. Levin, D. Svarts, and G. Ben-Dor. Study of the membrane effect on turbulent mixing measurements in shock tubes. *Shock Waves*, 10:241–251, 2000.

[18] M. H. Anderson, B. P. Puranik, J. G. Oakley, P. W. Brooks, and R. Bonazza. Shock tube investigation of hydrodynamic issues related to inertial confinement fusion. *Shock Waves*, 10(5):377–387, 2000.

[19] B. P. Puranik, J. G. Oakley, M. A. Anderson, and R. Bonazza. Experiments on the Richtmyer-Meshkov instability II: Nonlinear evolution of a membraneless single-mode

sinusoidal interface. University of Wisconsin Fusion Technology Institute, UWFDM-1172, September 2001.

[20] Lord Rayleigh. Investigation of the character of the equilibrium of an incompressible heavy fluid of variable density. *Scientific Papers, V. II*, pages 200–207, 1964. Dover Pub., NY, reprinted the 1900 papers.

[21] U. Alon, J. Hecht, D. Ofer, and D. Shvarts. Power laws and similarity of Rayleigh-Taylor and Richtmyer-Meshkov mixing fronts at all density ratios. *Phys. Rev. Let.*, 74(4):534–537, 1995.

[22] K. I. Read. Experimental investigation of turbulent mixing by Rayleigh-Taylor instability. *Physica 12D*, pages 45–58, 1984.

[23] O. Sadot, L. Erez, U. Alon, D. Oron, L. A. Levin, G. Erez, G. Ben-Dor, and D. Shvarts. Study of nonlinear evolution of single-mode and two-bubble interaction under Richtmyer-Meshkov instability. *Phys. Rev. Let.*, 80(8):1654–1657, 1998.